



Peptide and nucleic acid-directed self-assembly of cationic nanovehicles through giant unilamellar vesicle modification

Targetable nanocomplexes for *in vivo* nucleic acid delivery

Tagalakis, A. D.; Maeshima, R.; Yu-Wai-Man, C.; Meng, J.; Syed, F.; Wu, L. P.; Aldossary, A. M.; McCarthy, D.; Moghimi, S. M.; Hart, S. L.

Published in:
Acta Biomaterialia

DOI:
[10.1016/j.actbio.2017.01.048](https://doi.org/10.1016/j.actbio.2017.01.048)

Publication date:
2017

Document version
Peer reviewed version

Document license:
[CC BY-NC-ND](#)

Citation for published version (APA):
Tagalakis, A. D., Maeshima, R., Yu-Wai-Man, C., Meng, J., Syed, F., Wu, L. P., Aldossary, A. M., McCarthy, D., Moghimi, S. M., & Hart, S. L. (2017). Peptide and nucleic acid-directed self-assembly of cationic nanovehicles through giant unilamellar vesicle modification: Targetable nanocomplexes for *in vivo* nucleic acid delivery. *Acta Biomaterialia*, 51, 351-362. <https://doi.org/10.1016/j.actbio.2017.01.048>

Accepted Manuscript

Peptide and nucleic acid-directed self-assembly of cationic nanovehicles through giant unilamellar vesicle modification: targetable nanocomplexes for *in vivo* nucleic acid delivery

A.D. Tagalakis, R. Maeshima, C. Yu-Wai-Man, J. Meng, F. Syed, L.-P. Wu, A.M. Aldossary, D. McCarthy, S.M. Moghimi, S.L. Hart

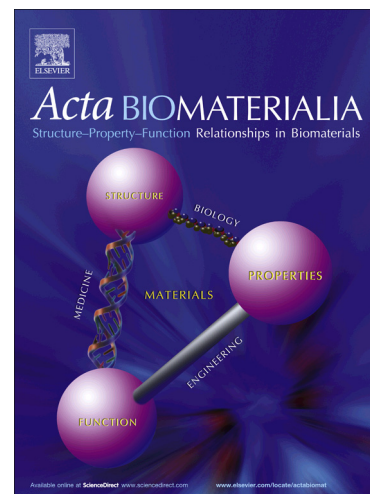
PII: S1742-7061(17)30057-0
DOI: <http://dx.doi.org/10.1016/j.actbio.2017.01.048>
Reference: ACTBIO 4683

To appear in: *Acta Biomaterialia*

Received Date: 10 September 2016
Revised Date: 16 January 2017
Accepted Date: 16 January 2017

Please cite this article as: Tagalakis, A.D., Maeshima, R., Yu-Wai-Man, C., Meng, J., Syed, F., Wu, L.-P., Aldossary, A.M., McCarthy, D., Moghimi, S.M., Hart, S.L., Peptide and nucleic acid-directed self-assembly of cationic nanovehicles through giant unilamellar vesicle modification: targetable nanocomplexes for *in vivo* nucleic acid delivery, *Acta Biomaterialia* (2017), doi: <http://dx.doi.org/10.1016/j.actbio.2017.01.048>

This is a PDF file of an unedited manuscript that has been accepted for publication. As a service to our customers we are providing this early version of the manuscript. The manuscript will undergo copyediting, typesetting, and review of the resulting proof before it is published in its final form. Please note that during the production process errors may be discovered which could affect the content, and all legal disclaimers that apply to the journal pertain.



Peptide and nucleic acid-directed self-assembly of cationic nanovehicles through giant unilamellar vesicle modification: targetable nanocomplexes for *in vivo* nucleic acid delivery

AD Tagalakis^{a,*}, R Maeshima^a, C Yu-Wai-Man^b, J Meng^a, F Syed^a, L-P Wu^c, AM Aldossary^a, D McCarthy^d, SM Moghimi^{c, e} & SL Hart^a

^aExperimental and Personalised Medicine Section, UCL Great Ormond Street Institute of Child Health, 30 Guilford Street, London, WC1N 1EH, UK

^bNational Institute for Health Research (NIHR) Biomedical Research Centre at Moorfields Eye Hospital NHS Foundation Trust and UCL Institute of Ophthalmology, 11-43 Bath Street, London, EC1V 9EL, UK

^cCentre for Pharmaceutical Nanotechnology and Nanotoxicology, Faculty of Health and Medical Sciences, University of Copenhagen, Universitetsparken 2, 2100 Copenhagen, Denmark

^dUCL School of Pharmacy, 29–39 Brunswick Square, London, WC1N 1AX, UK

^e School of Medicine, Pharmacy and Health, Durham University, Stockton-on-Tees TS17 6BH, UK

*Corresponding author: a.tagalakis@ucl.ac.uk

Keywords: GUV; vesicles; non-viral vectors; liposomes; peptide; lipopolyplexes; DNA; siRNA

ABSTRACT

One of the greatest challenges for the development of genetic therapies is the efficient targeted delivery of therapeutic nucleic acids. Towards this goal, we have introduced a new engineering initiative in self-assembly of biologically safe and stable nanovesicle complexes (~90-140 nm) derived from giant unilamellar vesicle (GUV) precursors and comprising plasmid DNA or siRNA and targeting peptide ligands. The biological performance of the engineered nanovesicle complexes were studied both *in vitro* and *in vivo* and compared with cationic liposome-based lipopolyplexes. Compared with cationic lipopolyplexes, nanovesicle complexes did not show advantages in transfection and cell uptake. However, nanovesicle complexes neither displayed significant cytotoxicity nor activated the complement system, which are advantageous for intravenous injection and tumour therapy. On intravenous administration into a neuroblastoma xenograft mouse model, nanovesicle complexes were found to distribute throughout the tumour interstitium, thus providing an alternative safer approach for future development of tumour-specific therapeutic nucleic acid interventions. On oropharyngeal instillation, nanovesicle complexes displayed better transfection efficiency than cationic lipopolyplexes. The technological advantages of nanovesicle complexes, originating from GUVs, over traditional cationic liposome-based lipopolyplexes are discussed.

1. Introduction

Formulations of cationic lipids that self-assemble into lipoplexes upon mixing with nucleic acids have received considerable attention. These non-viral vectors have recently become more popular with the development of small interfering RNA (siRNA)-mediated silencing and chemically-modified mRNA [1-4]. Nucleic acid therapy has great potential for the treatment of a wide range of diseases [5], however, only a small number of formulations used *in vitro*, make it to clinical trials as there are a number of barriers to *in vivo* delivery and transfection [4, 6]. Previously, we described the use of liposome-peptide receptor-targeted nanoparticles (RTNs) for both *in vitro* [7-11] and *in vivo* [12-18] nucleic acid delivery to various sites and targets in the body. These lipopolyplexes are capable of inducing nucleic acid compaction and their protection against premature degradation in biological fluids.

There is always a need to improve the performance of delivery vehicles and giant unilamellar vesicles (GUVs) have some interesting properties for the development of functional nucleic acid delivery systems with tunable properties [19, 20]. Earlier, DNA-directed self-assembly of GUVs has been shown, where DNA was introduced to vesicular surface by covalent conjugation [21-24]. These GUVs, also proved to be invaluable *in vitro* tools for the mechanistic understanding of complex and integrated biophysical and biomembrane processes [25-32]. Here, we exploit the bilayer properties of GUVs as the starting platform for self-assembly of a new generation of safe and stable lipid-peptide-nucleic acid transfectants with improved biological performance through the introduction of sugars for improved stabilization as well as targeting peptide ligands [20]. Indeed, the difference in density between the equiosmolar monosaccharidic intervesicular (external) and the disaccharidic intravesicular (internal) aqueous solutions offer vesicular stabilization and shape uniformity [33] as well as optical contrast. In addition, it is known that cationic transfectants can induce bioenergetic crisis, which dependent on cell type and mitochondrial polarization state it may initiate cell death [34]. The sugars associated with the engineered GUVs (e.g. glucose) could potentially help in re-establishing homeostasis with increased ATP synthesis, thereby overcoming cytotoxicity pertaining to cationic lipoplexes and lipopolyplexes.

GUVs carrying nucleic acids may exhibit limited cell uptake and transfection efficacy due to their large size compared with conventional large unilamellar vesicles [35]. Accordingly, we have introduced GUVs as precursors for generating vesicles in the nanoscale range

(hereinafter termed “nanovesicles”). Nanovesicles were complexed with nucleic acids (DNA or siRNA) and functionalized with different targeting peptides. The latter have included: 1) ME27, which contains the Arg-Gly-Asp (RGD) motif capable of targeting integrins and particularly $\alpha_v\beta_3$, $\alpha_v\beta_5$, and $\alpha_5\beta_1$ classes expressed in a wide range of tumours, 2) YGLPHKF (which is derived from peptide Y, a generic targeting peptide that works well across a range of tissues, including cells of neuronal origin) [8, 9] and closely resembles part of a targeting protein expressed by the intracellular pathogen *Legionella pneumophila* [36], and 3) peptide E, which has the SERSMNF motif that displays close similarity to receptor binding proteins of two intracellular pathogens, rhinovirus and *Listeria monocytogenes* [36]. Rhinoviruses bind the intercellular adhesion molecule-1 (ICAM-1) [37]. ICAM-1 is present in the airway epithelium and is upregulated in the inflamed epithelium as in cystic fibrosis [37, 38].

Collectively, our studies comprise biophysical characterization of targetable nanovesicle complexes as well as their improved biosafety in relevant *in vitro* and *in vivo* models compared with conventional cationic lipoplexes and lipopolyplexes.

2. Experimental section

2.1. Materials

1,2-di-O-octadecenyl-3-trimethylammonium propane (DOTMA) and 1,2-dioleoyl-*sn*-glycero-3-phosphoethanolamine (DOPE) were purchased from Avanti Polar Lipids, Inc. (Alabaster, AL, USA). Peptide Y (K16GACYGLPHKFCG) was synthesized by ChinaPeptides Co., Ltd. (Shanghai, People’s Republic of China), peptide E (K16GACSERSMNFCEG) was synthesized by Zinsser Analytics (Maidenhead, UK), peptide ME27 (K16RVRRGACRGDCLG) was synthesized by Alta Bioscience (Birmingham, UK) and the linear lysine peptide K16 was purchased from ImunnoKontakt (Abingdon, UK). Dy677 control siRNA (siRNA-Dy677) was purchased from GE Healthcare (Amersham, UK). Cy3-labelled control plasmid DNA (DNA-Cy3) was purchased from Cambridge Bioscience (Cambridge, UK). The plasmid pCI-Luc consists of the luciferase gene from pGL3 (Thermo Fisher Scientific, Hemel Hempstead, UK) sub-cloned into pCI (Promega Corporation, Fitchburg, WI, USA). The plasmid pEGFP-N1 (4.7

kb) containing the gene *GFP* was obtained from Clontech Laboratories, Inc. (Mountain View, CA, USA).

2.2. Nanovesicle formation from *GUV* precursors

DOTMA and DOPE were dissolved in chloroform to a concentration of 10 mg/mL. Lipids were mixed at a 1:1 molar ratio. The chloroform was evaporated in a rotary evaporator (BÜCHI Labortechnik AG, Flawil, Switzerland). The lipid film was dissolved in light mineral oil (catalog number: M5310; Sigma-Aldrich, Poole, UK) to a final concentration of 1.7 mg/mL by heating up to 50°C, sonicated for 30 min in an ultrasonic water bath (Jencons-PLS, Bedfordshire, UK) and incubated overnight at room temperature (RT). The lipid solution in mineral oil was then stored at -20°C prior to further use. For the DOTMA/DOPE (DD) liposome preparation, the lipid film was dissolved in water followed by sonication. For the nanovesicle (DOTMA/DOPE_{ves} or DD_{ves}) preparation, we used a modified version of the water/oil (W/O) emulsion transfer method [20, 26] described in detail by Hadorn et al. [23]. All solutions were prepared using Milli-Q water. Sucrose (99.5%) and glucose (99.0%) were purchased from Sigma-Aldrich (Poole, UK). The sucrose solution as well as the aqueous phase (glucose solution) was adjusted to 1000 mM (equiosmolar conditions) to avoid any osmotic pressure that would reduce vesicular stability. Consequently, the sucrose solution as well as the aqueous phase only differed in their densities.

The W/O emulsion was prepared in microtubes by adding 50 µL of the sucrose solution to 400 µL of the lipid solution prepared above and vigorously grated against a microtube rack for 3 min with force to aid emulsification. The intermediate phase was prepared in microtubes by adding 150 µL of the lipid solution to 300 µL of the aqueous phase and incubation at RT for 10 min. To generate the nanovesicles, the emulsion was then placed on top of the intermediate phase and centrifuged for 3 min at 1500g at RT. The oil was removed by aspiration and the pellet was resuspended in the osmotically-adjusted glucose (aqueous phase) and kept at 4°C.

To prevent the nanovesicles from adhering to surfaces, microscope slides and coverslips were treated with PlusOne Repel-Silane ES (GE Healthcare, Amersham, UK) in accordance with manufacturer's recommendation. Nanovesicle suspension (10 µL) was applied to a microscope slide and covered with a coverslip and then visualized (20x magnification) using an Olympus IX70 fluorescent microscope (Olympus Corporation, Tokyo, Japan).

2.3. Nanocomplex formation

Cationic receptor-targeted nanocomplex (RTN) formulations (at a weight ratio of 1:4:1, liposome or nanovesicle: peptide: DNA or siRNA) were made by first adding the peptide to the liposome or nanovesicle DOTMA/DOPE (DOTMA/DOPE and DOTMA/DOPE_{ves}, respectively), followed by addition of the DNA or siRNA with rapid mixing and incubation for 30 min at RT to allow for complex formation. The composition and terminology of the nanocomplexes (lipopolyplexes or nanovesicle complexes) are summarized in Table 1.

2.4. Size and zeta potential determinations

Nanocomplex preparations were diluted with distilled water to a final volume of 1 mL at a concentration of 5 µg/mL with respect to DNA or siRNA. They were then analyzed for size and electrophoretic mobility measurements using a Malvern Nano ZS (Malvern, UK). The following specifications were used: automatic sampling time of 10 measurements/sample, refractive index of 1.330 (water) and 1.340 (5% w/v glucose), dielectric constant 78.5 (water) and 77.37 (5% w/v glucose), viscosity 0.8872 cP (water) and 1.1450 cP (5% w/v glucose), and temperature of 25°C. DTS version 5.03, which was provided by the manufacturer, was used for data processing.

2.5. Heparin dissociation assay

DNA (0.2 µg) was mixed with PicoGreen reagent (1:150) (Invitrogen, Paisley, UK) at RT in Tris-EDTA buffer and the DNA/PicoGreen mixture was then formulated into nanocomplexes at a 1:4:1 weight ratio (liposome or nanovesicle: peptide: DNA) as described above. Heparin sulfate (Sigma-Aldrich, Poole, UK) was added to the PicoGreen-labelled nanocomplexes in a range of concentrations (0-2 U/mL). In each experiment, naked DNA stained with PicoGreen was used to normalize the PicoGreen signal detected from the nanocomplexes. Fluorescence was analyzed using a fluorescence plate reader, FLUOstar Optima (BMG Labtech, Aylesbury, UK).

2.6. Transmission electron microscopy (TEM)

For the electron microscopy investigations, the nanocomplexes were prepared as described above and were placed on a glow-discharged 300-mesh copper grid coated with a Formvar/carbon support film (Agar Scientific). After a few seconds, the grid was blotted with a filter paper. The sample was then negatively stained with 1% (w/v) uranyl acetate or 1% (w/v)

phosphotungstic acid, before blotting and then air-dried. Imaging was carried out under a Philips CM120 BioTwin Transmission Electron Microscope and operated at an accelerating voltage of 120 KV.

2.7 Cell culture

Murine Neuro-2A and human Kelly neuroblastoma cell lines were obtained from the American Type Culture Collection (Teddington, UK). Neuro-2A cells were maintained in Dulbecco's Minimal Essential Medium (DMEM; Invitrogen, Paisley, UK) supplemented with 10% (v/v) FBS, 1% (v/v) non-essential amino acids, and 1% (v/v) sodium pyruvate. Kelly cells were cultured in RPMI1640+GlutaMAX (Invitrogen, Paisley, UK) with 10% (v/v) FBS, 25 mM HEPES and 100 U/mL Penicillin/Streptomycin. The human bronchial epithelial cells 16HBE14o- (shortened to HBE) were provided by D. Gruenert, (San Francisco, CA, USA) and were cultured in Eagle's Minimal Essential Medium with HEPES modification (Sigma, Poole, UK), 10% (v/v) FCS and 2 mM L-glutamine. All cells were maintained in a humidified atmosphere of 95% air and 5% CO₂ at 37°C.

2.8 DNA transfection

Neuro-2A cells were seeded in 96-well plates at 2×10^4 cells per well 24 h prior to transfection. Following the removal of growth medium, 200 µL of complexes in OptiMEM containing 0.25 µg of plasmid DNA were added to the cells in replicates of six. Plates were centrifuged at 400g for 5 min and incubated for 4 h at 37°C, then transfection medium was replaced by the complete growth medium and incubated for a further 24 h. Luciferase expression was measured in cell lysates with a luciferase assay (Promega, Southampton, UK) in a FLUOstar OPTIMA luminometer (BMG Labtech, Aylesbury, UK). The amount of protein present in each sample was determined with the Bio-Rad protein assay reagent (Bio-Rad Laboratories, Hemel Hempstead, UK) in a FLUOstar OPTIMA luminometer. Luciferase activity was expressed as relative light units per milligram of protein (RLU/mg). Each measurement was performed in groups of six.

The same protocol was used for transfections with eGFP plasmid DNA with the only difference being that the cells following transfection were incubated for 48 h at 37°C. They were firstly imaged (20× magnification) using an Olympus IX70 fluorescent microscope (Olympus,

Southend-on-Sea, UK) and then prepared for flow cytometry by detaching cells from the wells with 50 μ L Trypsin-EDTA (Sigma-Aldrich, Poole, UK) and re-suspending them with 150 μ L Dulbecco's phosphate-buffered saline (DPBS; Sigma-Aldrich, Poole, UK). Cells were acquired with a BD FACSAArray flow cytometer (BD Biosciences, Oxford, UK) and analyzed with FlowJo software v. 8.8.3 (Tree Star Inc., Ashland, Oregon, USA).

2.9 Flow cytometry analysis

After 4 h or 24 h of transfection with different nanocomplexes, the Neuro-2A cells were washed with PBS twice and then trypsinized and re-suspended in culture medium in a 96-well plate. The uptake of the siRNA-Dy677 or DNA-Cy3 by cells in each well was analyzed using BD FACSCalibur™. Non-transfected cells were used to set the negative control gate. Acquired data were analyzed using FlowJo software v. 8.8.3 (Tree Star Inc., Ashland, Oregon, USA) to determine the percentage of the Dy677-positive or Cy3-positive cells in each treatment group.

2.10 In-cell Western analysis

After 4, 24 and 48 h post transfection of Neuro-2A cells with different siRNA-Dy677 nanocomplexes, the 96-well plate was washed twice with PBS and scanned by the Odyssey Clx infrared imaging system (LI-COR Biosciences, Cambridge, UK) and the intensity of the 700 nm fluorescent channel for each well was determined using image studio software 3.1.4.

2.11 Viable cell assay

Viable cell assay was assessed in 96-well plates using the CellTiter 96 Aqueous One Solution Cell Proliferation Assay (Promega, Southampton, UK). Neuro-2A cells were seeded and transfected as above. After 24 h the medium was substituted for a growth medium containing 20 μ L of the CellTiter 96 Aqueous One Solution reagent. Finally, after incubation for 2 h, the absorbance at 490 nm was measured on a FLUOstar Optima spectrophotometer (BMG Labtech, Aylesbury, UK). Viable cells for each formulation treatment were expressed as a percentage of the viable control cells.

2.12 Complement Activation assays

Details for human serum preparation, characterization and functional assessment of

complement pathways were described previously [39-41]. To measure complement activation *in vitro*, we determined nanocomplex-induced rise of serum complement activation products C5a and sC5b-9 using respective ELISA kits (Quidel, San Diego) according to the manufacturer's protocol as described earlier [39-41]. Complement activation was initiated by adding the appropriate quantities of nanocomplexes (in 10 μ L) to undiluted human serum (40 μ L) in Eppendorf tubes in a shaking water bath at 37°C for 30 min. Reactions were terminated by addition of ice-cold sample-diluent provided in the assay kit containing 25mM EDTA. Nanocomplexes were removed by centrifugation, and complement activation products were measured in ELISA kits. Control serum incubations contained buffers that were used for liposome suspension. Zymosan was prepared as described before [41] and was used as a positive control for generating C5a and sC5b-9 at a concentration of 0.2 mg/mL.

2.13 *In vivo experiments*

Female C57Bl6 mice were purchased from Charles River (Margate, UK). All procedures were approved by UCL animal care policies and were carried out under Home Office Licenses issued in accordance with the United Kingdom Animals (Scientific Procedures) Act 1986 (UK). DOTMA/DOPE lipopolyplexes and DOTMA/DOPE_{ves} nanovesicle complexes were prepared at a weight ratio of 1:4:1 (lipid: peptide: DNA) as described previously [18] at a final plasmid DNA concentration of 0.29 mg/mL. 6-week old female C57Bl6 mice were instilled oropharyngeally with nanocomplexes in 55 μ L (made in 5% glucose, v/v) containing 16 μ g pCI-Luc, with untreated mice used as controls. 24 h following instillation, the mice were culled and their lungs extracted and snap frozen. Lungs were defrosted on ice, submerged in reporter gene assay lysis buffer (Roche, Basel, Switzerland), homogenized with a Precellys24 tissue homogenizer (Stretton Scientific, Stretton, Derbyshire, UK) and then centrifuged at 14,170g for 10 min at 4°C. The supernatant was removed and centrifuged for a further 10 min at 4°C and then used in luciferase assays. Results were expressed as relative luminescence units per milligram of protein (RLU/mg).

Female NOD-SCID gamma (NSG) mice (Charles River, Margate, UK), 6 to 8 week old, were injected subcutaneously in the right posterior flank with 3×10^6 human neuroblastoma Kelly cells. After approximately 2 weeks, when tumours had reached 8–10 mm in size, 100 μ L

of RTN complexes made in 5% (v/v) glucose and containing 16 µg of siRNA-Dy677 were injected into the lateral tail vein. Experiments were performed with replicates of 3 mice. 24 hours after injection, the mice were killed and tumours and organs (lung, liver, heart, kidneys and spleen) were resected and imaged using an IVIS Lumina Series III imaging system (PerkinElmer, Seer Green, UK). The images were processed using the Living Image software (PerkinElmer, Seer Green, UK). The tumours were then placed in 4% (w/v) paraformaldehyde (PFA) for 3 h followed by overnight incubation in 15% (w/v) sucrose/PBS and then a brief wash in 50% (v/v) ethanol and stored briefly in 70% (v/v) ethanol till ready for dissection.

2.14 Preparation of frozen tissue sections

Freshly dissected tissue was placed onto a pre-labelled tissue base mold. Tissue block was covered with cryo-embedding media OCT (Leica microsystems, Milton Keynes, UK). Base mold containing tissue block was snap frozen in isopentane (VWR International, Lutterworth, UK), pre-chilled in liquid nitrogen and then transferred to a cryotome cryostat, which was pre cooled to -20°C. 10 µm tissue sections were prepared using the cryotome and mounted on the Superfrost Plus glass slides (Fisher Scientific UK, Loughborough, UK). The sections were dried at RT and then stored at -80°C until utilized.

2.15 Staining of frozen sections

Tissue sections were rinsed in PBS briefly to remove any media components and fixed in pre-cooled (-20°C) acetone for 10-15 min. Next, tissue sections were rinsed three times in PBS and stained with DAPI for 15 min at RT in dark. Finally, tissue sections were washed three times in PBS and sections were mounted using ProLong® Gold antifade mountant (Thermo Fisher Scientific, Hemel Hempstead, UK). Micrographs were taken using Leica upright fluorescence (Leica DFC310 FX) at 200x magnification.

2.16 Statistical analysis

The data presented in this study are expressed as the mean ± standard deviation (SD) and were analyzed using a two-tailed, unpaired Student's *t*-test or one-way analysis of variance and Bonferroni's post hoc analysis, where applicable.

3. Results

3.1. Biophysical characterization. The sizes and zeta potentials (Fig. 1A and Fig. S1) of nanovesicles, cationic liposomes, nanovesicle complexes and lipopolyplexes were determined first. Nanovesicles were considerably larger than their liposomal counterparts (557.0 ± 82.5 nm vs 76.1 ± 0.9 nm, respectively) consisting of two particle populations (Fig. S1) and had comparable average zeta potential values (66.9 ± 1.7 mV for nanovesicles vs 70.9 ± 2.4 mV for liposomes, respectively). These nanovesicles were capable of forming complexes with peptide and nucleic acid (DNA or siRNA) of 89.6 ± 1.3 nm, when mixed with DNA, or under 140 nm, when mixed with siRNA, respectively (Fig. 1A and Fig. S1). There was no statistical difference in the size of the nanocomplexes, however, LYD_{ves} had the least cationic surface charge among all nanocomplexes (zeta potential of 26.2 ± 0.4 mV for LYD_{ves} vs 47.7 ± 3.0 mV for LYD).

Negative staining transmission electron microscopy (TEM) was used to further characterize nanovesicles (Fig. 1B) and nanovesicle complexes (LYD_{ves}; Fig. 1C). Nanovesicles and nanovesicle complexes were predominantly spherical, however, some rod-shaped objects were also present (in LYD_{ves}; Fig. 1C). The majority of the spherical entities observed by TEM for each formulation were in similar size ranges determined by dynamic light scattering (DLS). DOTMA/DOPE liposomes and LYD lipopolyplexes were also visualized (Fig. S2) and they formed some discrete spherical particles with most being aggregated in clusters. These clusters may have been generated during sample preparation and dehydration processes for TEM.

The ability of nanocomplexes to package DNA efficiently and to dissociate following heparin challenge was assessed (Fig. 1D). PicoGreen-labelled DNA was formulated into cationic LYD and LYD_{ves}. Packaging was inferred from fluorescence quenching compared with free DNA as 100%. The packaging efficiency refers to the extent of nucleic acid protection. Therefore, the higher the packaging efficiency, the better the protection of the nucleic acid cargo. Both formulations resulted in high packaging efficiency: 81% for LYD lipopolyplexes compared with 94% for LYD_{ves} nanovesicle complexes. In addition, they had a different heparin release profile. LYD achieved 50% dissociation at 0.41 U/mL heparin, whereas LYD_{ves} achieved 50% dissociation at 0.84 U/mL heparin, thus making the latter less responsive to polyanions.

3.2. Cellular uptake and targeting specificity of siRNA-containing nanocomplexes. Next, we

determined cellular uptake of Dy677-labelled siRNA nanocomplexes following transfection of Neuro-2A cells in comparison with liposomes. The following complexes were used: nanovesicle complexes made from fresh nanovesicles and incorporating targeting peptides (LYR_{ves-new} and LMER_{ves-new}) or a non-targeting peptide (LK16R_{ves-new}), nanovesicle complexes made with nanovesicles previously stored for 1 year at 4°C and incorporating targeting peptides (LYR_{ves-old1} and LMER_{ves-old1}), lipopolyplexes with targeting peptides (LYR and LMER) or non-targeting peptide (LK16R), peptide/siRNA complexes (Y/ siRNA-Dy677 and ME27/ siRNA-Dy677), liposome/siRNA (LR) or nanovesicle/siRNA (LR_{ves-new}). Two complementary methods were used for analysis: in-cell Western analysis of the siRNA-Dy677 uptake (Fig. 2A-B) and measurement of the fluorescent intensity of the Dy677 (which reflects the uptake level of the siRNA). The results show a time-dependent uptake of nanocomplexes. In particular, lipopolyplexes had a higher and statistically significant uptake than their respective nanovesicle complex counterparts at 4 h (LYR_{ves} uptake was 35.4% vs 53.8% for LYR, $p<0.001$), but this was not significant at later time points. Similar observations were made with formulations incorporating the targeting peptide ME27. The nanocomplexes that were made with nanovesicles stored for one year in the fridge had approximately a 2.5-fold increased size (215-240 nm) compared with their fresh counterparts and this might explain why they showed less uptake than freshly made counterparts. Other comparisons that were significant for all time points were those of LR (liposome/siRNA) or LR_{ves} (nanovesicle/siRNA) formulations, which displayed inferior uptake to lipopolyplexes ($p<0.001$). Peptide/siRNA (PR) formulations also displayed significantly less cell uptake compared with lipopolyplexes ($p<0.001$). Particularly, the formulations with the targeted peptides resulted in a much higher uptake than those with non-targeted peptides ($p<0.001$ for all comparisons), however, this effect was more pronounced with the nanovesicle complexes. For example at 24 h, LYR_{ves} resulted in approximately 10-fold higher uptake than LK16R_{ves}, which was considerably higher than the difference in uptake of LYR, which in turn was 2.6-fold higher than that of LK16R.

Flow cytometry analysis (Fig. 2C), showed a similar uptake pattern to that of in-cell Western analysis at 4 h post transfection. The comparisons described above as being significant (Fig. 2A-B) were also significant in Fig. 2C. For example, the targeted formulations resulted in a much higher uptake than their non-targeted counterparts ($p<0.001$ for all comparisons), however again this effect was more pronounced with the nanovesicle complexes. FACS analysis was also

performed to investigate the uptake of Cy3-labelled DNA nanocomplexes in Neuro-2A cells. The trend was the same as the one found for siRNA uptake; again there was no statistical difference between nanovesicle complexes and lipopolyplexes at 24 h and the use of targeting peptides resulted in higher uptake than non-targeting formulations (Fig. S3). However, PR and peptide/DNA (PD) complexes showed a significantly different nucleic acid uptake profile. For example at 4 h post-transfection, PD complexes (Fig. S3) achieved 22.5% uptake, which was significantly more than the 4.1% seen with the PR formulations (Fig. 2C; $p < 0.05$).

3.3. *In vitro* transfection efficiencies. Nanocomplexes were formulated and used for transfection of Neuro-2A and HBE cells (Fig. 3). LMED formulations were significantly better in transfection than the LMED_{ves} ($p < 0.05$) in Neuro-2A cells (Fig. 3A), however, this difference was not statistically significant for LYD and LYD_{ves} nanocomplexes in HBE cells (Fig. 3B). Importantly, the receptor-targeted formulations showed considerable differences in transfection efficiency compared with the non-targeted formulations. Targeted lipopolyplexes LMED (Neuro-2A cells) and LYD (HBE cells) resulted in a 3.6-fold and a 4.3-fold enhancement of transfection compared with non-targeting LK16D ($p < 0.001$ for both Neuro-2A and HBE cells), whereas the vesicular targeted formulations LMED_{ves} (Neuro-2A cells) and LYD_{ves} (HBE cells) resulted in a 10.5-fold and 8.9-fold ($p < 0.001$ for both Neuro-2A and HBE cells) increase in transfection efficiency compared with non-targeting LK16D_{ves}, respectively.

The transfection efficiency was further evaluated with the plasmid expressing enhanced green fluorescent protein (GFP) in Neuro-2A cells 48 h after transfection. Fluorescent microscopy images of LMED_{ves} (Fig. 3C) and LMED (Fig. 3D) nanocomplexes provided evidence of the high transfection efficiency of both formulations. Flow cytometry analysis of GFP transfections was then performed (Fig. 4) and showed that $28.6 \pm 1.9\%$ and $33.5 \pm 2.2\%$ of cells expressed GFP following transfection with LMED_{ves} and LMED, respectively ($p < 0.05$).

3.4. Complement activation assay and cell viability. We challenged undiluted human serum with LYD and LYD_{ves} formulations and measured the two pathway-independent soluble end-point complement activation products C5a and sC5b-9, respectively [39, 42]. The complement system is a key effector of both innate and cognate immunity recognizing danger signals through pattern recognition [43]. C5a is an anaphylatoxin and chemoattractant agent,

whereas soluble sC5b-9 is a measure of whole complement activation. The results in Fig. 5A show that neither formulations elevated sC5b-9 levels above the background compared on the basis of equivalent surface area. On the other hand, both formulations caused very small increases of serum C5a levels (Fig. 5B). For comparison zymosan treatment induced massive rises of C5a and sC5b-9 levels above background (201.3 ± 10.1 ng/mL C5a and 31.7 ± 1.6 μ g/mL sC5b-9, respectively). On the basis of our findings, our formulations were poor activators of the complement system and could be used for intravenous applications. Indeed, the extent of complement activation by these preparations was considerably lower than PEGylated regulatory approved liposomes (Doxil®) on equivalent surface area (46 cm^2) basis (8560 ± 108.1 ng/mL sC5b-9) [44].

The cell viability assessment showed no particular differences between nanocomplexes, which included lipopolyplexes and nanovesicle complexes (Fig. 5C). However, the cationic liposomes DOTMA/DOPE (from either a fresh or an older batch) were significantly more cytotoxic (65% viable cells) compared with untreated controls ($p < 0.001$ for both batches). On the contrary, all the batches of the nanovesicles DOTMA/DOPE_{ves} did not induce any apparent cytotoxicity.

3.5. *In vivo* lung delivery and tumour distribution. We further determined whether the *in vitro* results translate to *in vivo* performance. Firstly, LED (size: 95.3 ± 1.4 nm; ζ potential 54.5 ± 1.3 mV) and LED_{ves} (size: 96.3 ± 0.5 nm; ζ potential 43.5 ± 0.6 mV) nanocomplexes were delivered to the airways of murine lungs (Fig. 6). 24 h after administration, luciferase assay was performed on lung extracts. The mean luciferase expression from LED_{ves} was higher than that of LED (6160 RLU/mg protein for LED_{ves} vs 4596 RLU/mg protein for LED), but this was not statistically significant.

Finally, we investigated whether LMER_{ves} nanocomplexes can be delivered to tumours following systemic administration in xenograft mouse models of neuroblastoma. 24 h after intravenous administration, the organs and the tumours were removed and imaged using the IVIS III system for siRNA-Dy677 distribution. The LMER_{ves} nanocomplexes showed high retention in tumours (17.5% of the initial injected dose; the radiant efficiency of the initial dose was measured at 1.9×10^{10} photons $\text{s}^{-1} \text{ cm}^{-2}$ steradian $^{-1}$ per $\mu\text{W cm}^{-2}$), while leaving other normal tissues with extremely low (heart, liver, kidneys and spleen) or moderate uptake (lung; 5.2% of

the initial injected dose) (Fig. 7A-B). The fluorescent radiant efficiency was 3.39-fold higher in tumours than in the lungs (Fig. S4, $p < 0.01$). Immunostaining of the tumours (Fig. 7C-H) revealed that the siRNA-Dy677 was strongly present throughout the tumour mass and the staining was very intense in mice injected with targeted LMER_{ves}, whereas the intracellular fluorescence signals were not detected in the tumour tissues collected from control untreated mice.

4. Discussion

In this study, we replaced the liposomal component of lipopolyplexes, which was derived through sonication of multi-lamellar vesicles [8, 15-18, 45], with GUVs as initial templates for vector assembly (nanovesicles and nanovesicle complexes). Following further processing, these preparations were characterized and compared with sonicated liposomes. These modifications resulted in formation of large unilamellar vesicles, with the majority being less than 1 μm . The engineered vesicles comprise of a bilayer that isolates the aqueous lumen of the intermediate vesicles loaded with sucrose from the external hosting glucose solution [19, 46, 47]. When complexed with peptide ligands and nucleic acids, we were able to produce nanovesicle complexes that were less than 140 nm. The electrostatic forces involved between nanovesicles, peptides and nucleic acids most likely play a role in compaction processes and, hence, the observed reduction in size of the nanovesicle complexes compared with native nanovesicles. Indeed, the size of the nanocomplexes should preferentially be less than 200 nm to allow for efficient internalization through different endocytic processes as well as for tumour targeting [48].

While extracellular stability is an essential requirement for formulation of an efficient nucleic acid delivery system, effective transfection is also influenced by the extent of cargo release intracellularly. For instance, cationic lipopolyplexes may interact favourably with actin during internalization causing destabilization and partial release of nucleic acids directly into the cytoplasm [49, 50]. To compare particle stability and nucleic acid dissociation, nanocomplexes were incubated with heparin, which mimics actin [9, 49]. Both types of nanocomplexes achieved approximately 65% maximum release at a heparin concentration of 2 U/mL, thus suggesting their suitability for nucleic acid delivery and release.

Next we compared cell uptake of the engineered formulations. The higher positive charge of the lipopolyplexes compared with nanovesicles could explain the differences in cell uptake, either through better plasma membrane destabilization (causing direct nucleic acid release into the cytoplasm) and/or improved interaction with anionic components of cell surface proteoglycans [51]. Furthermore, it has been shown that shape is an important factor in cellular uptake and that rods may enter cells more readily than spheres under static conditions and particularly from a side-on mode of contact with plasma membrane [52, 53]. Indeed, nanovesicle particles were mostly spherical in shape, whereas lipopolyplexes contained a high number of rods and torroids [9, 16, 45, 54] as well as particle clusters, which could explain their higher uptake. Our results further showed that the nanocomplexes that were made with nanovesicles after prolonged storage had larger size and reduced cell uptake. It is likely that fusion processes may have caused vesicular destabilization and partial release of complexed nucleic acids prior to cell incubation.

The initial barriers to transfection are cell binding and uptake [54, 55]. Differences in efficiencies of these two processes could potentially explain the different transfection efficiencies of the nanocomplexes. LPD complexes had similar biophysical characteristics with LPD_{ves}, but displayed improved cellular uptake and this may explain the differences in their transfection efficiencies, providing that cell viability is not compromised. Our results show that plasmid DNA in LPD_{ves} nanovesicle complexes is more tightly packaged (94%) than in LPD lipopolyplexes (81%; $p < 0.001$), however, DNA was more easily released from LPD lipopolyplexes than from LPD_{ves} nanovesicle complexes. Thus LPD having a greater cell uptake, while resulting in better DNA release within the cell, achieves the greater transfection efficiencies observed. The targeted formulations were more efficient than their non-targeting counterparts due to the presence of the targeting peptide, which resulted in a higher uptake in the cells as corroborated in Fig. 2.

Although nanovesicle complexes did not show advantages in transfection and cell uptake compared with lipopolyplexes, they were considerably less cytotoxic than their liposomal counterparts. This is most likely due to their lesser cationic charge. In addition, cells may use the glucose that was present in the nanovesicle complexes (e.g., DOTMA/DOPE_{ves}) to maintain oxidative phosphorylation and ATP synthesis. It is well documented [56, 57] that cationic liposomes are cytotoxic and this could explain the reduced cell viability observed in our assay

for DOTMA/DOPE. The LPD lipopolyplexes were also found to be significantly less cytotoxic than the cationic DOTMA/DOPE liposome, which implies that DNA or siRNA may have sequestered the cationic lipid reducing its damaging effect on cells.

Our *in vivo* studies further showed the suitability of LED_{ves} in nucleic acid delivery. For instance, following oropharyngeal administration nanovesicle complexes were more effective in nucleic acid delivery and transfection than lipopolyplexes (LED). This observation contrasted the *in vitro* findings where the lipopolyplexes showed superiority. We have previously shown that nanocomplexes target mainly the airway epithelia [18], thus a plausible explanation for these differences may arise from a relatively higher destabilization of LED at the apical surface of the lung cells compared with the sugar-containing LED_{ves}. As for tumour targeting, we used a near-infrared fluorescent probe, Dy677, which results in low autofluorescence and scattering of light and enables good tissue penetration of light, which is ideal for *in vivo* imaging [58]. Our nanocomplexes, following intravenous administration, were mainly localized to tumours and showed less deposition to the lungs. Others have also shown that at 24 h following intravenous administration, cationic nanoparticles coupled to $\alpha\beta 3$ ligands were mainly expressing luciferase in tumours with minimal activity detected in the lung and heart and none in other organs [59]. This distribution pattern is very important as the nanocomplexes were able to largely avoid the reticuloendothelial system (RES), which is the major clearance mechanism of nanoparticles from the circulation [60]. This might be attributed to the targeting peptide utilized here and to the enhanced permeation and retention effect (EPR) and the leakiness of the tumour neovasculature in our *in vivo* model [61]. Another contributing factor may be poor complement opsonization of the engineered nanocomplexes and hence their poor recognition by macrophages of the RES, thereby allowing more nanoparticles to reach tumours. These results collectively indicate that the targeted nanovesicle complexes could efficiently deliver siRNA to the tumour tissue, and thus might have potential applications in therapeutic oncology. Finally, considering the high level of nanovesicle complex accumulation in tumour interstitium, their poor complement activating nature is clinically advantageous. Indeed, intratumoural complement activation has been suggested to accelerate tumour growth [62, 63].

5. Conclusion

Giant liposomes have been used for biophysical investigations, namely the interaction of cytoskeleton proteins with membranes, the dynamic structures of biomembranes and the change of liposomal shapes [64-66]. These vesicles have the advantage over traditional smaller liposomal preparations of being easier to prepare in small quantities and by high throughput procedures [19, 23, 26, 47, 67, 68]. Here, we initially modified the procedure of making GUVs that resulted in nanovesicles of less than 1 μm in size and then for the first time, we reported the development of nanovesicle complexes using these nanovesicles (derived from GUV precursors). These engineered vesicles exhibited good transfection efficiency, however, unlike conventional cationic lipoplexes, nanovesicles and nanovesicle complexes neither exhibited considerable cytotoxicity nor activated the complement system. These observations are of importance, since nanovesicle complexes were able to deliver nucleic acids to both lung and tumour tissues *in vivo*. Nanovesicle complexes therefore represent a promising tool for improving our arsenal of safer non-viral vectors for site-specific delivery of therapeutic nucleic acids.

Acknowledgement

We would like to thank the Maeshima Medical Office, Action Medical Research and Cystic Fibrosis Trust for funding this work. This work was further supported by the National Institute for Health Research Biomedical Research Centre at Great Ormond Street Hospital for Children NHS Foundation Trust and University College London. We would like to thank Dr Boenzli for helpful discussions and for proofreading the manuscript.

References

- [1] N. Pardi, S. Tuyishime, H. Muramatsu, K. Kariko, B. L. Mui, Y. K. Tam, T. D. Madden, M. J. Hope, D. Weissman. Expression kinetics of nucleoside-modified mRNA delivered in lipid nanoparticles to mice by various routes, *J. Control. Release* 217 (2015) 345-351.
- [2] S. C. Semple, A. Akinc, J. X. Chen, A. P. Sandhu, B. L. Mui, C. K. Cho, D. W. Y. Sah, D. Stebbing, E. J. Crosley, E. Yaworski, I. M. Hafez, J. R. Dorkin, J. Qin, K. Lam, K. G. Rajeev, K. F. Wong, L. B. Jeffs, L. Nechev, M. L. Eisenhardt, M. Jayaraman, M. Kazem, M. A. Maier, M. Srinivasulu, M. J. Weinstein, Q. M. Chen, R. Alvarez, S. A. Barros, S. De, S. K. Klimuk, T. Borland, V. Kosovrasti, W. L. Cantley, Y. K. Tam, M. Manoharan, M. A. Ciufolini, M. A.

- Tracy, A. de Fougerolles, I. MacLachlan, P. R. Cullis, T. D. Madden, M. J. Hope. Rational design of cationic lipids for siRNA delivery, *Nat. Biotechnol.* 28 (2010) 172-176.
- [3] A. D. Tagalakakis, I. A. Diakonov, I. R. Graham, K. A. Heald, J. D. Harris, J. V. Mulcahy, G. Dickson, J. S. Owen. Apolipoprotein E delivery by peritoneal implantation of encapsulated recombinant cells improves the hyperlipidaemic profile in apoE-deficient mice, *BBA-Mol. Cell. Biol. L.* 1686 (2005) 190-199.
- [4] H. Yin, R. L. Kanasty, A. A. Eltoukhy, A. J. Vegas, J. R. Dorkin, D. G. Anderson. Non-viral vectors for gene-based therapy, *Nat. Rev. Genet.* 15 (2014) 541-555.
- [5] C. Sheridan. Gene therapy finds its niche, *Nat. Biotechnol.* 29 (2011) 121-128.
- [6] Y. Zhang, A. Satterlee, L. Huang. In vivo gene delivery by nonviral vectors: overcoming hurdles?, *Mol. Ther.* 20 (2012) 1298-1304.
- [7] A. Kwok, D. McCarthy, S. L. Hart, A. D. Tagalakakis. Systematic Comparisons of Formulations of Linear Oligolysine Peptides with siRNA and Plasmid DNA, *Chem. Biol. Drug Des.* 87 (2016) 747-763.
- [8] A. D. Tagalakakis, L. He, L. Saraiva, K. T. Gustafsson, S. L. Hart. Receptor-targeted liposome-peptide nanocomplexes for siRNA delivery, *Biomaterials* 32 (2011) 6302-6315.
- [9] A. D. Tagalakakis, L. Saraiva, D. McCarthy, K. T. Gustafsson, S. L. Hart. Comparison of Nanocomplexes with Branched and Linear Peptides for SiRNA Delivery, *Biomacromolecules* 14 (2013) 761-770.
- [10] A. Weng, M. D. I. Manunta, M. Thakur, R. Gilabert-Oriol, A. D. Tagalakakis, A. Eddaoudi, M. M. Munye, C. A. Vink, B. Wiesner, J. Eichhorst, M. F. Melzig, S. L. Hart. Improved intracellular delivery of peptide- and lipid-nanoplexes by natural glycosides, *J. Control. Release* 206 (2015) 75-90.
- [11] C. Yu-Wai-Man, A. D. Tagalakakis, M. D. Manunta, S. L. Hart, P. T. Khaw. Receptor-targeted liposome-peptide-siRNA nanoparticles represent an efficient delivery system for MRTF silencing in conjunctival fibrosis, *Sci. Rep.* 6 (2016) 21881.
- [12] G. D. Kenny, C. Villegas-Llerena, A. D. Tagalakakis, F. Campbell, K. Welser, M. Botta, A. B. Tabor, H. C. Hailes, M. F. Lythgoe, S. L. Hart. Multifunctional receptor-targeted nanocomplexes for magnetic resonance imaging and transfection of tumours, *Biomaterials* 33 (2012) 7241-7250.
- [13] Q. H. Meng, S. Irvine, A. D. Tagalakakis, R. J. McNulty, J. R. McEwan, S. L. Hart. Inhibition of neointimal hyperplasia in a rabbit vein graft model following non-viral transfection

with human iNOS cDNA, *Gene Ther.* 20 (2013) 979-986.

[14] M. M. Munye, A. D. Tagalakakis, J. L. Barnes, R. E. Brown, R. J. McAnulty, S. J. Howe, S. L. Hart. Minicircle DNA Provides Enhanced and Prolonged Transgene Expression Following Airway Gene Transfer, *Sci. Rep.* 6 (2016) 23125.

[15] A. D. Tagalakakis, S. M. Grosse, Q. H. Meng, M. F. M. Mustapa, A. Kwok, S. E. Salehi, A. B. Tabor, H. C. Hailes, S. L. Hart. Integrin-targeted nanocomplexes for tumour specific delivery and therapy by systemic administration, *Biomaterials* 32 (2011) 1370-1376.

[16] A. D. Tagalakakis, G. D. Kenny, A. S. Bienemann, D. McCarthy, M. M. Munye, H. Taylor, M. J. Wyatt, M. F. Lythgoe, E. A. White, S. L. Hart. PEGylation improves the receptor-mediated transfection efficiency of peptide-targeted, self-assembling, anionic nanocomplexes, *J. Control. Release* 174 (2014) 177-187.

[17] A. D. Tagalakakis, D. H. D. Lee, A. S. Bienemann, H. Y. Zhou, M. M. Munye, L. Saraiva, D. McCarthy, Z. X. Du, C. A. Vink, R. Maeshima, E. A. White, K. Gustafsson, S. L. Hart. Multifunctional, self-assembling anionic peptide-lipid nanocomplexes for targeted siRNA delivery, *Biomaterials* 35 (2014) 8406-8415.

[18] A. D. Tagalakakis, R. J. McAnulty, J. Devaney, S. E. Bottoms, J. B. Wong, M. Elbs, M. J. Writer, H. C. Hailes, A. B. Tabor, C. O'Callaghan, A. Jaffe, S. L. Hart. A receptor-targeted nanocomplex vector system optimized for respiratory gene transfer, *Mol. Ther.* 16 (2008) 907-915.

[19] M. Hadorn, E. Boenzli, K. T. Sorensen, D. De Lucrezia, M. M. Hanczyc, T. Yomo. Defined DNA-mediated assemblies of gene-expressing giant unilamellar vesicles, *Langmuir* 29 (2013) 15309-15319.

[20] S. Pautot, B. J. Frisken, D. A. Weitz. Engineering asymmetric vesicles, *Proc. Natl. Acad. Sci. U S A* 100 (2003) 10718-10721.

[21] P. A. Beales, J. Nam, T. K. Vanderlick. Specific adhesion between DNA-functionalized "Janus" vesicles: size-limited clusters, *Soft Matter* 7 (2011) 1747-1755.

[22] M. Hadorn, E. Boenzli, M. M. Hanczyc. Specific and Reversible DNA-Directed Self-Assembly of Modular Vesicle-Droplet Hybrid Materials, *Langmuir* 32 (2016) 3561-3566.

[23] M. Hadorn, P. Eggenberger Hotz. DNA-mediated self-assembly of artificial vesicles, *PLoS One* 5 (2010) e9886.

[24] L. Parolini, B. M. Moggetti, J. Kotar, E. Eiser, P. Cicuta, L. Di Michele. Volume and

- porosity thermal regulation in lipid mesophases by coupling mobile ligands to soft membranes, Nat. Commun. 6 (2015) 5948.
- [25] A. S. Cans, M. Andes-Koback, C. D. Keating. Positioning lipid membrane domains in giant vesicles by micro-organization of aqueous cytoplasm mimic, J. Am. Chem. Soc. 130 (2008) 7400-7406.
- [26] M. Hadorn, E. Boenzli, P. E. Hotz. A quantitative analytical method to test for salt effects on giant unilamellar vesicles, Sci. Rep. 1 (2011) 168.
- [27] R. Kwok, E. Evans. Thermoelasticity of large lecithin bilayer vesicles, Biophys. J. 35 (1981) 637-652.
- [28] M. Mally, J. Majhenc, S. Svetina, B. Zeks. The response of giant phospholipid vesicles to pore-forming peptide melittin, Biochim. Biophys. Acta 1768 (2007) 1179-1189.
- [29] C. Mauroy, T. Portet, M. Winterhalder, E. Bellard, M. C. Blache, J. Teissie, A. Zumbusch, M. P. Rols. Giant lipid vesicles under electric field pulses assessed by non invasive imaging, Bioelectrochemistry 87 (2012) 253-259.
- [30] S. L. Veatch, O. Soubias, S. L. Keller, K. Gawrisch. Critical fluctuations in domain-forming lipid mixtures, Proc. Natl. Acad. Sci. U S A 104 (2007) 17650-17655.
- [31] Y. Yu, J. A. Vroman, S. C. Bae, S. Granick. Vesicle budding induced by a pore-forming peptide, J. Am. Chem. Soc. 132 (2010) 195-201.
- [32] J. Zhou, A. L. Loftus, G. Mulley, A. T. Jenkins. A thin film detection/response system for pathogenic bacteria, J. Am. Chem. Soc. 132 (2010) 6566-6570.
- [33] R. Dimova, S. Aranda, N. Bezlyepkina, V. Nikolov, K. A. Riske, R. Lipowsky. A practical guide to giant vesicles. Probing the membrane nanoregime via optical microscopy, J. Phys. Condens. Matter 18 (2006) S1151-1176.
- [34] A. Hall, L. Parhamifar, M. K. Lange, K. D. Meyle, M. Sanderhoff, H. Andersen, M. Roursgaard, A. K. Larsen, P. B. Jensen, C. Christensen, J. Bartek, S. M. Moghimi. Polyethylenimine architecture-dependent metabolic imprints and perturbation of cellular redox homeostasis, Biochim. Biophys. Acta 1847 (2015) 328-342.
- [35] L. R. Montes, A. Alonso, F. M. Goni, L. A. Bagatolli. Giant unilamellar vesicles electroformed from native membranes and organic lipid mixtures under physiological conditions, Biophys. J. 93 (2007) 3548-3554.
- [36] M. J. Writer, B. Marshall, M. A. Pilkington-Miksa, S. E. Barker, M. Jacobsen, A. Kritz, P.

- C. Bell, D. H. Lester, A. B. Tabor, H. C. Hailes, N. Klein, S. L. Hart. Targeted gene delivery to human airway epithelial cells with synthetic vectors incorporating novel targeting peptides selected by phage display, *J. Drug Target.* 12 (2004) 185-193.
- [37] J. Bella, P. R. Kolatkar, C. W. Marlor, J. M. Greve, M. G. Rossmann. The structure of the two amino-terminal domains of human ICAM-1 suggests how it functions as a rhinovirus receptor and as an LFA-1 integrin ligand, *Proc. Natl. Acad. Sci. U S A* 95 (1998) 4140-4145.
- [38] S. C. Chan, D. K. Shum, G. L. Tipoe, J. C. Mak, E. T. Leung, M. S. Ip. Upregulation of ICAM-1 expression in bronchial epithelial cells by airway secretions in bronchiectasis, *Respir. Med.* 102 (2008) 287-298.
- [39] S. M. Moghimi, I. Hamad, T. L. Andresen, K. Jorgensen, J. Szebeni. Methylation of the phosphate oxygen moiety of phospholipid-methoxy(polyethylene glycol) conjugate prevents PEGylated liposome-mediated complement activation and anaphylatoxin production, *FASEB J.* 20 (2006) 2591-2593.
- [40] A. J. Andersen, J. T. Robinson, H. Dai, A. C. Hunter, T. L. Andresen, S. M. Moghimi. Single-walled carbon nanotube surface control of complement recognition and activation, *ACS Nano* 7 (2013) 1108-1119.
- [41] N. K. Banda, G. Mehta, Y. Chao, G. K. Wang, S. Inturi, L. Fossati-Jimack, M. Botto, L. P. Wu, S. M. Moghimi, D. Simberg. Mechanisms of complement activation by dextran-coated superparamagnetic iron oxide (SPIO) nanoworms in mouse versus human serum, *Part. Fibre Toxicol.* 11 (2014)64.
- [42] I. D. Azmi, L. Wu, P. P. Wibroe, C. Nilsson, J. Ostergaard, S. Sturup, B. Gammelgaard, A. Urtti, S. M. Moghimi, A. Yaghmur. Modulatory effect of human plasma on the internal nanostructure and size characteristics of liquid-crystalline nanocarriers, *Langmuir* 31 (2015) 5042-5049.
- [43] S. M. Moghimi, A. J. Andersen, D. Ahmadvand, P. P. Wibroe, T. L. Andresen, A. C. Hunter. Material properties in complement activation, *Adv. Drug Deliv. Rev.* 63 (2011) 1000-1007.
- [44] P. P. Wibroe, D. Ahmadvand, M. A. Oghabian, A. Yaghmur, S. M. Moghimi. An integrated assessment of morphology, size, and complement activation of the PEGylated liposomal doxorubicin products Doxil(R), Caelyx(R), DOXOrubicin, and SinaDoxosome, *J. Control. Release* 221 (2016) 1-8.

- [45] A. D. Tagalakakis, S. Castellaro, H. Y. Zhou, A. Bienemann, M. M. Munye, D. McCarthy, E. A. White, S. L. Hart. A method for concentrating lipid peptide DNA and siRNA nanocomplexes that retains their structure and transfection efficiency, *Int. J. Nanomed.* 10 (2015) 2673-2683.
- [46] T. Bhatia, P. Husen, J. Brewer, L. A. Bagatolli, P. L. Hansen, J. H. Ipsen, O. G. Mouritsen. Preparing giant unilamellar vesicles (GUVs) of complex lipid mixtures on demand: Mixing small unilamellar vesicles of compositionally heterogeneous mixtures, *Biochim. Biophys. Acta* 1848 (2015) 3175-3180.
- [47] M. Hadorn, E. Boenzli, P. Eggenberger Hotz, M. M. Hanczyc. Hierarchical unilamellar vesicles of controlled compositional heterogeneity, *PLoS One* 7 (2012) e50156.
- [48] H. Gao, W. Shi, L. B. Freund. Mechanics of receptor-mediated endocytosis, *Proc. Natl. Acad. Sci. U S A* 102 (2005) 9469-9474.
- [49] M. Mannisto, M. Reinisalo, M. Ruponen, P. Honkakoski, M. Tammi, A. Urtti. Polyplex-mediated gene transfer and cell cycle: effect of carrier on cellular uptake and intracellular kinetics, and significance of glycosaminoglycans, *J. Gene Med.* 9 (2007) 479-487.
- [50] C. Schweiger, R. Hartmann, F. Zhang, W. J. Parak, T. H. Kissel, P. Rivera Gil. Quantification of the internalization patterns of superparamagnetic iron oxide nanoparticles with opposite charge, *J. Nanobiotechnol.* 10 (2012) 28.
- [51] X. X. Zhang, T. J. McIntosh, M. W. Grinstaff. Functional lipids and lipoplexes for improved gene delivery. *Biochimie* 2012;94:42-58.
- [52] S. E. Gratton, P. A. Ropp, P. D. Pohlhaus, J. C. Luft, V. J. Madden, M. E. Napier, J. M. DeSimone. The effect of particle design on cellular internalization pathways, *Proc. Natl. Acad. Sci. U S A* 105 (2008) 11613-11618.
- [53] J. M. Williford, J. L. Santos, R. Shyam, H. Q. Mao. Shape Control in Engineering of Polymeric Nanoparticles for Therapeutic Delivery, *Biomater. Sci.* 3 (2015) 894-907.
- [54] Z. X. Du, M. M. Munye, A. D. Tagalakakis, M. D. I. Manunta, S. L. Hart. The Role of the Helper Lipid on the DNA Transfection Efficiency of Lipopolyplex Formulations, *Sci. Rep.* 4 (2014) 7107.
- [55] M. M. Munye, J. Ravi, A. D. Tagalakakis, D. McCarthy, M. G. Ryadnov, S. L. Hart. Role of liposome and peptide in the synergistic enhancement of transfection with a lipopolyplex vector, *Sci. Rep.* 5 (2015) 9292.
- [56] B. Ballarin-Gonzalez, K. A. Howard. Polycation-based nanoparticle delivery of RNAi

- therapeutics: adverse effects and solutions, *Adv. Drug Deliv. Rev.* 64 (2012) 1717-1729.
- [57] K. Romoren, B. J. Thu, N. C. Bols, O. Evensen. Transfection efficiency and cytotoxicity of cationic liposomes in salmonid cell lines of hepatocyte and macrophage origin, *Biochim. Biophys. Acta* 1663 (2004) 127-134.
- [58] X. B. Xiong, A. Lavasanifar. Traceable multifunctional micellar nanocarriers for cancer-targeted co-delivery of MDR-1 siRNA and doxorubicin, *ACS Nano* 5 (2011) 5202-5213.
- [59] J. D. Hood, M. Bednarski, R. Frausto, S. Guccione, R. A. Reisfeld, R. Xiang, D. A. Cheresh. Tumor regression by targeted gene delivery to the neovasculature, *Science* 296 (2002) 2404-2407.
- [60] S. D. Li, L. Huang. Nanoparticles evading the reticuloendothelial system: role of the supported bilayer, *Biochim. Biophys. Acta* 1788 (2009) 2259-2266.
- [61] W. L. Monsky, D. Fukumura, T. Gohongi, M. Ancukiewicz, H. A. Weich, V. P. Torchilin, F. Yuan, R. K. Jain. Augmentation of transvascular transport of macromolecules and nanoparticles in tumors using vascular endothelial growth factor, *Cancer Res.* 59 (1999) 4129-4135.
- [62] M. M. Markiewski, R. A. DeAngelis, F. Benencia, S. K. Ricklin-Lichtsteiner, A. Koutoulaki, C. Gerard, G. Coukos, J. D. Lambris. Modulation of the antitumor immune response by complement, *Nat. Immunol.* 9 (2008) 1225-1235.
- [63] S. M. Moghimi. Cancer nanomedicine and the complement system activation paradigm: Anaphylaxis and tumour growth, *J. Control. Release* 190 (2014) 556-562.
- [64] M. Honda, K. Takiguchi, S. Ishikawa, H. Hotani. Morphogenesis of liposomes encapsulating actin depends on the type of actin-crosslinking, *J. Mol. Biol.* 287 (1999) 293-300.
- [65] J. Kas, E. Sackmann. Shape transitions and shape stability of giant phospholipid vesicles in pure water induced by area-to-volume changes, *Biophys. J.* 60 (1991) 825-844.
- [66] O. Sandre, L. Moreaux, F. Brochard-Wyart. Dynamics of transient pores in stretched vesicles, *Proc. Natl. Acad. Sci. U S A* 96 (1999) 10591-10596.
- [67] S. H. C. Askes, N. L. Mora, R. Harkes, R. I. Koning, B. Koster, T. Schmidt, A. Kros, S. Bonnet. Imaging the lipid bilayer of giant unilamellar vesicles using red-to-blue light upconversion, *Chem. Commun.* 51 (2015) 9137-9140.
- [68] S. Pautot, B. J. Frisken, D. A. Weitz. Production of unilamellar vesicles using an inverted emulsion, *Langmuir* 19 (2003) 2870-2879.

Name	Components
LYD (lipopolyplex)	DOTMA/DOPE/Peptide Y/DNA
LED (lipopolyplex)	DOTMA/DOPE/Peptide E/DNA
LMED (lipopolyplex)	DOTMA/DOPE/Peptide ME27/DNA
LK16D (lipopolyplex)	DOTMA/DOPE/Peptide K16/DNA
LYD _{ves} (nanovesicle complex)	DOTMA/DOPE nanovesicle/Peptide Y/DNA
LED _{ves} (nanovesicle complex)	DOTMA/DOPE nanovesicle/Peptide E/DNA
LMED _{ves} (nanovesicle complex)	DOTMA/DOPE nanovesicle/Peptide ME27/DNA
LK16D _{ves} (nanovesicle complex)	DOTMA/DOPE nanovesicle/Peptide K16/DNA
LYR (lipopolyplex)	DOTMA/DOPE/Peptide Y/siRNA
LMER (lipopolyplex)	DOTMA/DOPE/Peptide ME27/siRNA
LYR _{ves} (nanovesicle complex)	DOTMA/DOPE nanovesicle/Peptide Y/siRNA
LMER _{ves} (nanovesicle complex)	DOTMA/DOPE nanovesicle/Peptide ME27/siRNA

Table 1. Terminology of nanocomplexes (lipopolyplexes or nanovesicle complexes).

FIGURE LEGENDS

Fig. 1. Biophysical characteristics of nanovesicles, liposomes, nanovesicle complexes and lipopolyplexes (A) Size and surface charge measurements of cationic liposomes, nanovesicles, nanovesicle complexes and lipopolyplexes. Particle size was measured by dynamic light scattering. DD=DOTMA/DOPE, LYD=DOTMA/DOPE/Peptide Y/DNA, LYR=DOTMA/DOPE/Peptide Y/siRNA, DD_{ves}= DOTMA/DOPE nanovesicles, LYD_{ves}= DOTMA/DOPE nanovesicle/Peptide Y/DNA and LYR_{ves}= DOTMA/DOPE nanovesicle/Peptide Y/siRNA. (B) Negative staining TEM with 1% (w/v) uranyl acetate was used to visualize DOTMA/DOPE nanovesicles. Scale Bar= 2 μ m. (C) Negative staining TEM with 1% (w/v) uranyl acetate was used to visualize LYD_{ves} nanovesicle complexes. Scale Bar= 500 nm. (D) The dissociation properties of nanocomplexes LYD and LYD_{ves} were investigated. PicoGreen fluorescence of complexes, after incubation with heparin (0-2 U/mL), was expressed as a percentage of relative fluorescence units (RFU) relative to free DNA. All experiments were repeated at least 3 times.

Fig. 2. In-cell Western and flow cytometry analysis of the siRNA-Dy677 uptake of different nanocomplexes. Neuro-2A cells were transfected with different nanocomplexes and 4 h (A) or 24 h (B) later the plates were scanned for in-cell Western analysis. The plates are shown in the left panel. The graphs (right panel) show the relative fluorescence units (RFU) of each formulation to that of the naked siRNA, which is set at 1. A1-A6= LYR_{ves-new}, A7-A12= LYR, B1-B6= LMER_{ves-new}, B7-B12= LMER, C1-C6= LYR_{ves-old1}, C7-C12= LMER_{ves-old1}, D1-D6= LK16R, D7-D12= LK16R_{ves-new}, E1-E6= LR, E7-E12= LR_{ves-new}, F1-F6= DOTMA/DOPE_{ves-new}, F7-F12= DOTMA/DOPE, G1-G6= peptide Y/siRNA-Dy677, G7-G12= peptide ME27/siRNA-Dy677, H1-H6=siRNA-Dy677, H7-H12= control untransfected cells. Ves-old1 refers to nanovesicles made one year earlier and stored at 4°C and ves-new refers to freshly made nanovesicles. (C) The uptake of siRNA-containing nanocomplexes following transfection of Neuro-2A cells was measured 4 h post-transfection by flow cytometry. In all the graphs each column represents the mean \pm SD from six wells. Asterisks indicate comparison of specific formulations with statistical significance (***, $p < 0.001$).

Fig. 3. *In vitro* transfections of nanovesicle complexes and lipopolyplexes. (A) Nanocomplexes LMED_{ves} and LMED (with targeting peptide ME27) and LK16D_{ves} and LK16D (with non-targeting peptide K16) were used in luciferase transfections in Neuro-2A cells (B) Nanocomplexes LYD_{ves} and LYD (with targeting peptide Y) and LK16D_{ves} and LK16D (with non-targeting peptide K16) were used in luciferase transfections in HBE cells. The cells were assessed for luciferase expression 24 h later. Each column represents the mean \pm SD from six wells, and the experiment was repeated 3 times. Asterisks indicate comparison of specific formulations with statistical significance (*, $p < 0.05$; ***, $p < 0.001$). (B) (C-D) GFP transfection efficiency of the LMED_{ves} and the LMED nanocomplexes. Two formulations, LMED_{ves} nanovesicle complexes (C) and LMED lipopolyplexes (D) were used to transfect Neuro-2A cells. GFP expression was observed by epifluorescence microscopy 48 h later (representative cells are shown in phase-contrast on the left and transfected cells appear green on the right images; Scale Bar = 100 μ m). Peptide ME27 was used for all formulations.

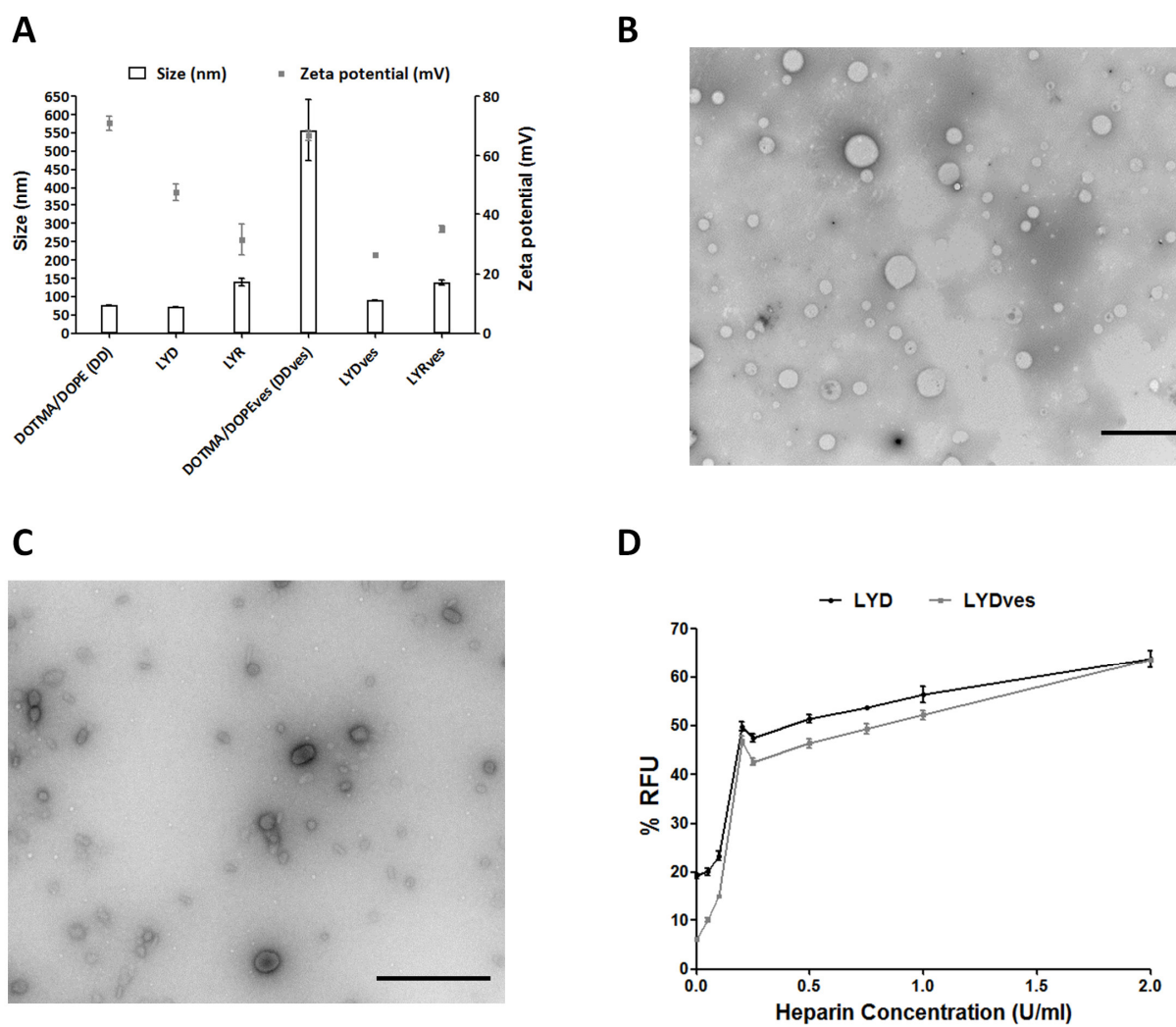
Fig. 4. Flow cytometry analysis of GFP expression in Neuro-2A cells. The intensity of GFP expression was evaluated at 48 h following transfection. (A) Control untransfected cells. (B) Cells transfected with LMED_{ves} nanovesicle complexes. (C) Cells transfected with LMED lipopolyplexes. FL1= fluorescence intensity, SSC= side scatter. Each experiment was performed in triplicate wells.

Fig. 5. Complement activation assays and cell viability show a lack of cytotoxicity. (A) Quantification of complement activation product of sC5b-9 in human serum after incubation of different concentration of nanocomplexes. Blank (PBS) and positive control (200 μ g/mL Zymosan, sC5b-9: 31678 ng/mL serum) were tested during the experiment, as were glucose (used in LYD_{ves}) and water (used in LYD). (B) Quantification of complement activation product of C5a in human serum after incubation of different concentration of nanocomplexes. Blank (PBS) and positive control (200 μ g/mL Zymosan, C5a: 201 ng/mL serum) were tested during the experiment, as were glucose (used in LYD_{ves}) and water (used in LYD). Asterisks indicate comparisons of specific formulations with statistical significance (*, $p < 0.05$; **, $p < 0.01$; ***, $p < 0.001$). (C) Viability of Neuro-2A cells following transfection for 24 h with different

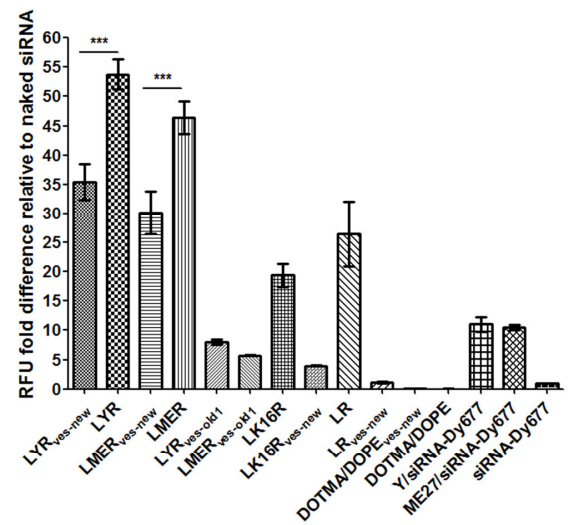
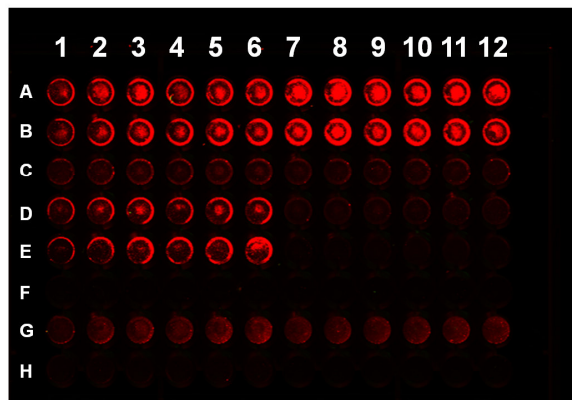
nanocomplexes. Viability values were normalized to the untransfected control cells. All transfections were performed in groups of six. Asterisks indicate comparisons of specific formulations to the control untransfected cells with statistical significance (***, $p < 0.001$). DD=DOTMA/DOPE, LYD_{old} =DOTMA/DOPE liposome one year old/peptide Y/DNA, LYD_{new} =DOTMA/DOPE fresh liposome/peptide Y/DNA, $LYD_{ves-old1}$ = DOTMA/DOPE nanovesicles 1 year old/peptide Y/DNA, $LYD_{ves-old2}$ = DOTMA/DOPE nanovesicles 6 months old/peptide Y/DNA, $LYD_{ves-new}$ = DOTMA/DOPE fresh nanovesicle/peptide Y/DNA, $LD_{ves-old1}$ =DOTMA/DOPE nanovesicles 1 year old/DNA, $LD_{ves-new}$ =DOTMA/DOPE fresh nanovesicle/DNA, PD=peptide Y/DNA, LYR_{ves} =DOTMA/DOPE fresh nanovesicle/peptide Y/siRNA.

Fig. 6. Transgene expression following *in vivo* transfections of mice lungs. Luciferase activity in mice lungs was detected 24 h following oropharyngeal instillation of LED_{ves} (nanovesicle complexes) or LED lipopolyplexes. Values are background subtracted and the bar represents mean RLU/mg.

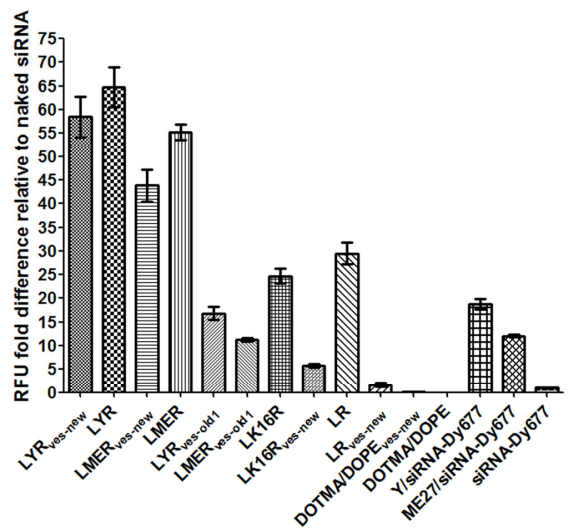
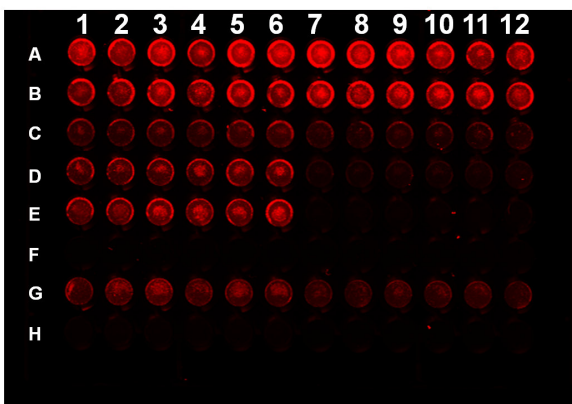
Fig. 7. Tumour uptake of formulations following intravenous administration. 24 h later the mice were culled (n=3 per group) and tumours and organs were extracted and imaged for fluorescence. (A) organs (heart, lung, liver, kidneys, spleen) and tumour of a mouse that received $LMER_{ves}$ (DOTMA/DOPE nanovesicle/peptide ME27/siRNA-Dy677) nanovesicle complexes and (B) mice tumours: control tumour (mouse was not injected) and tumour from a mouse that received $LMER_{ves}$ nanovesicle complexes. The fluorescence signal was also investigated in histological sections of tumours of control mice (C-E) or from mice following tail-vein injections of $LMER_{ves}$ nanovesicle complexes (F-H). The tumours were removed 24 h after the injection and the fluorescence recorded. The cell nuclei were stained with DAPI (blue) and the siRNA-Dy677 in red. (C, F) DAPI staining, (D, G) siRNA-Dy677 and (E, H) merged images. Scale Bar = 50 μ m.



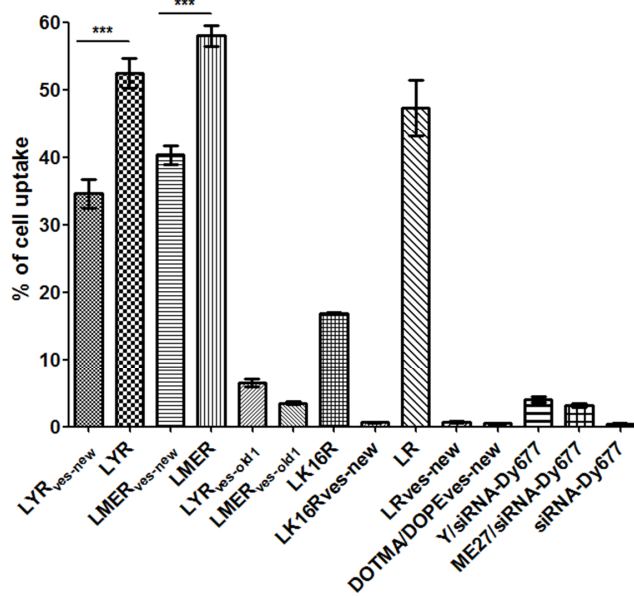
A

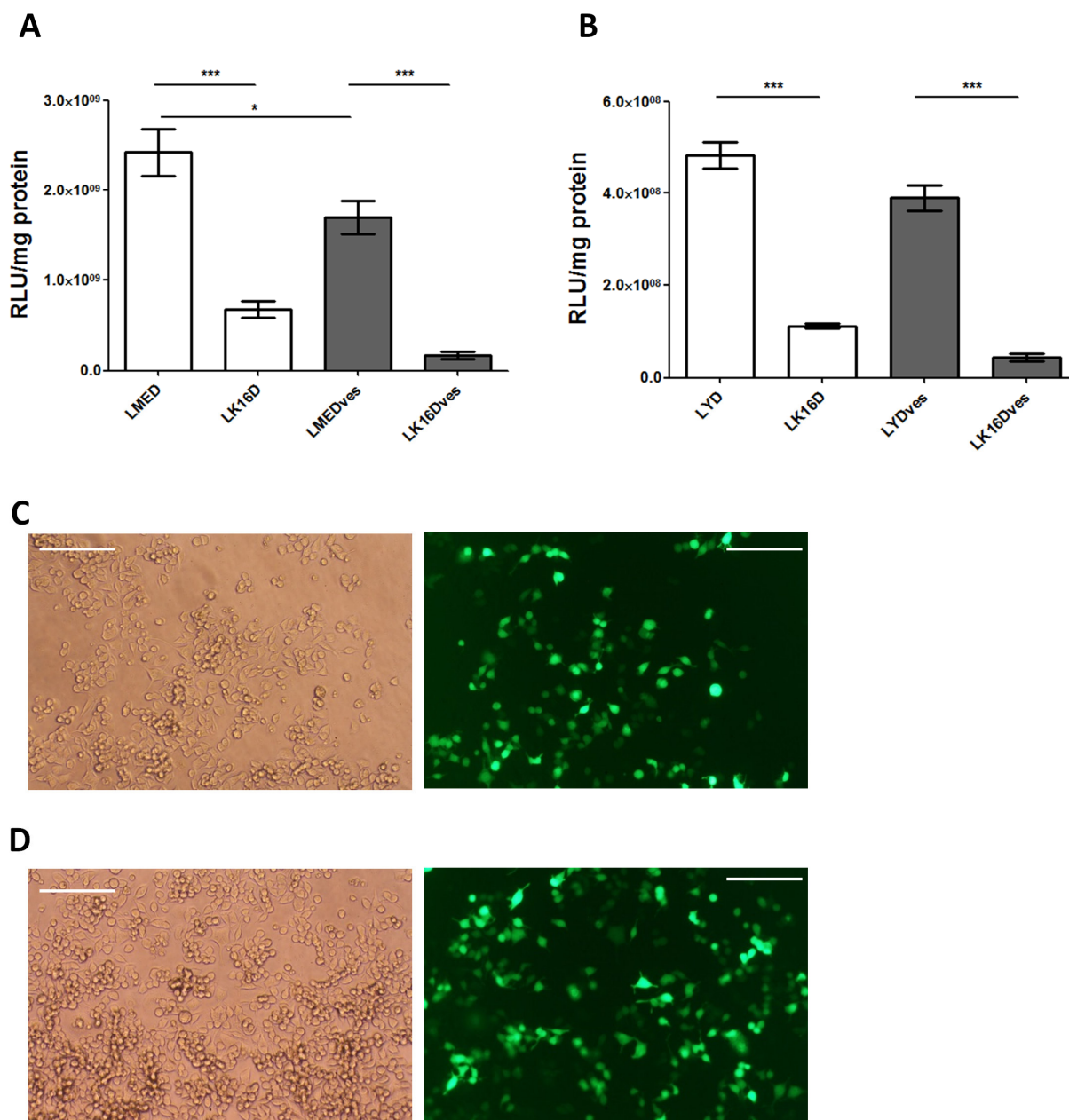


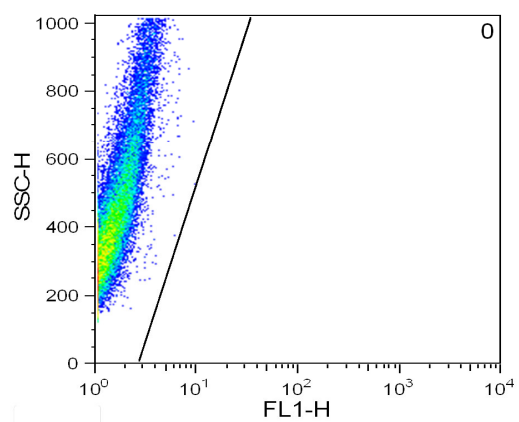
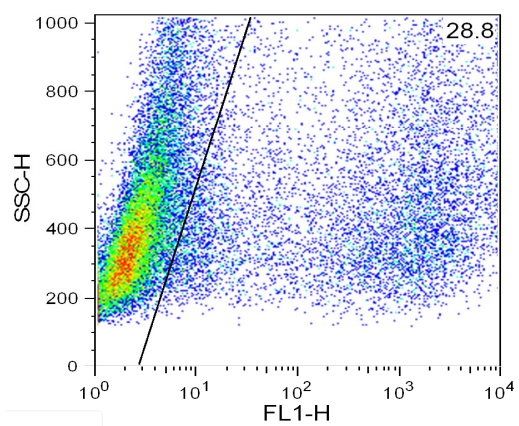
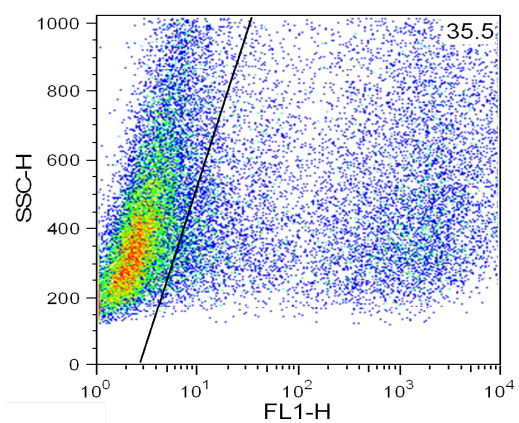
B

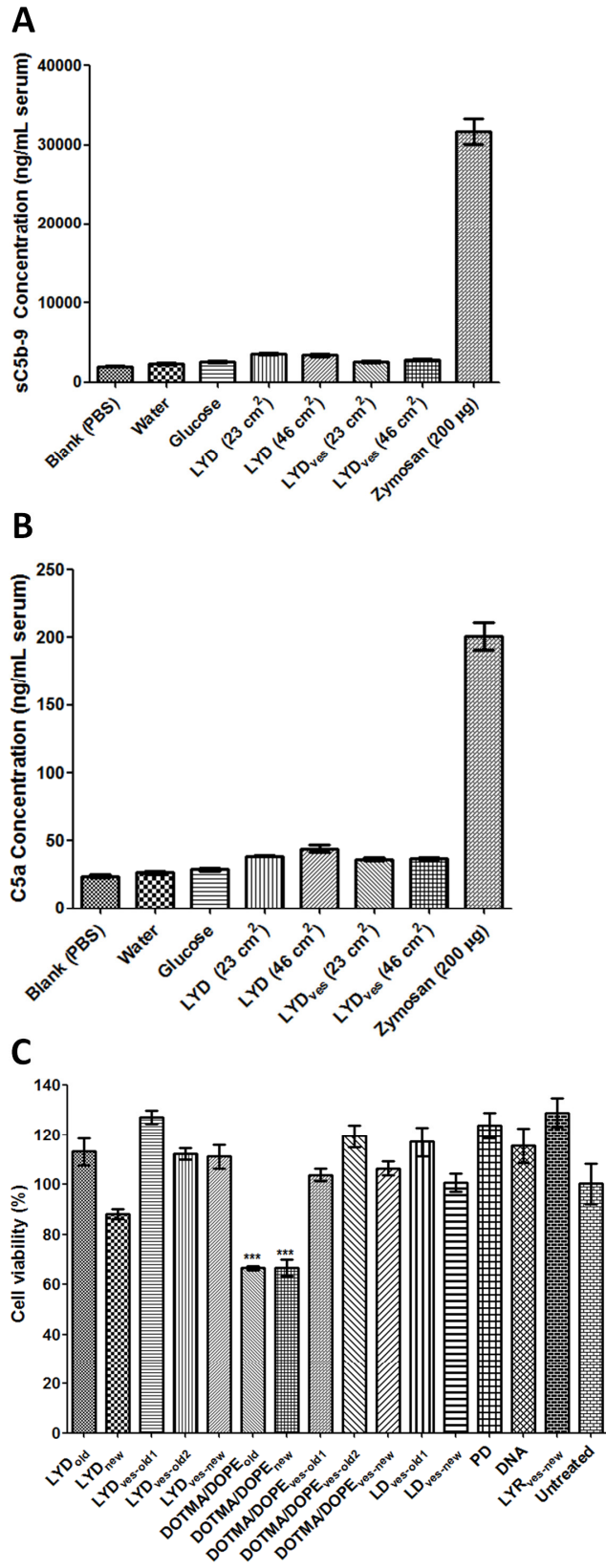


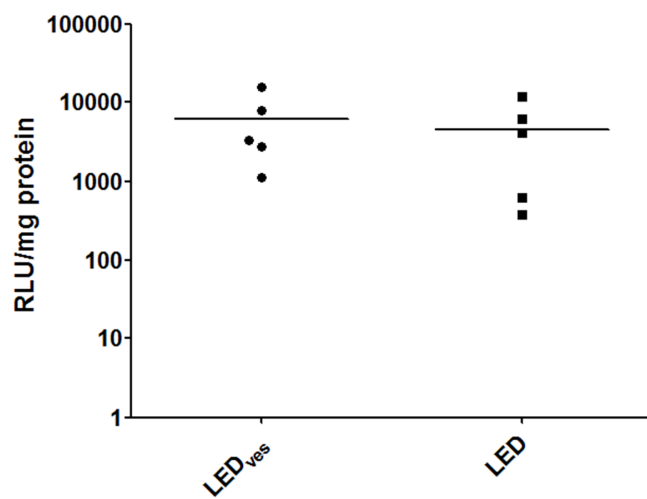
C

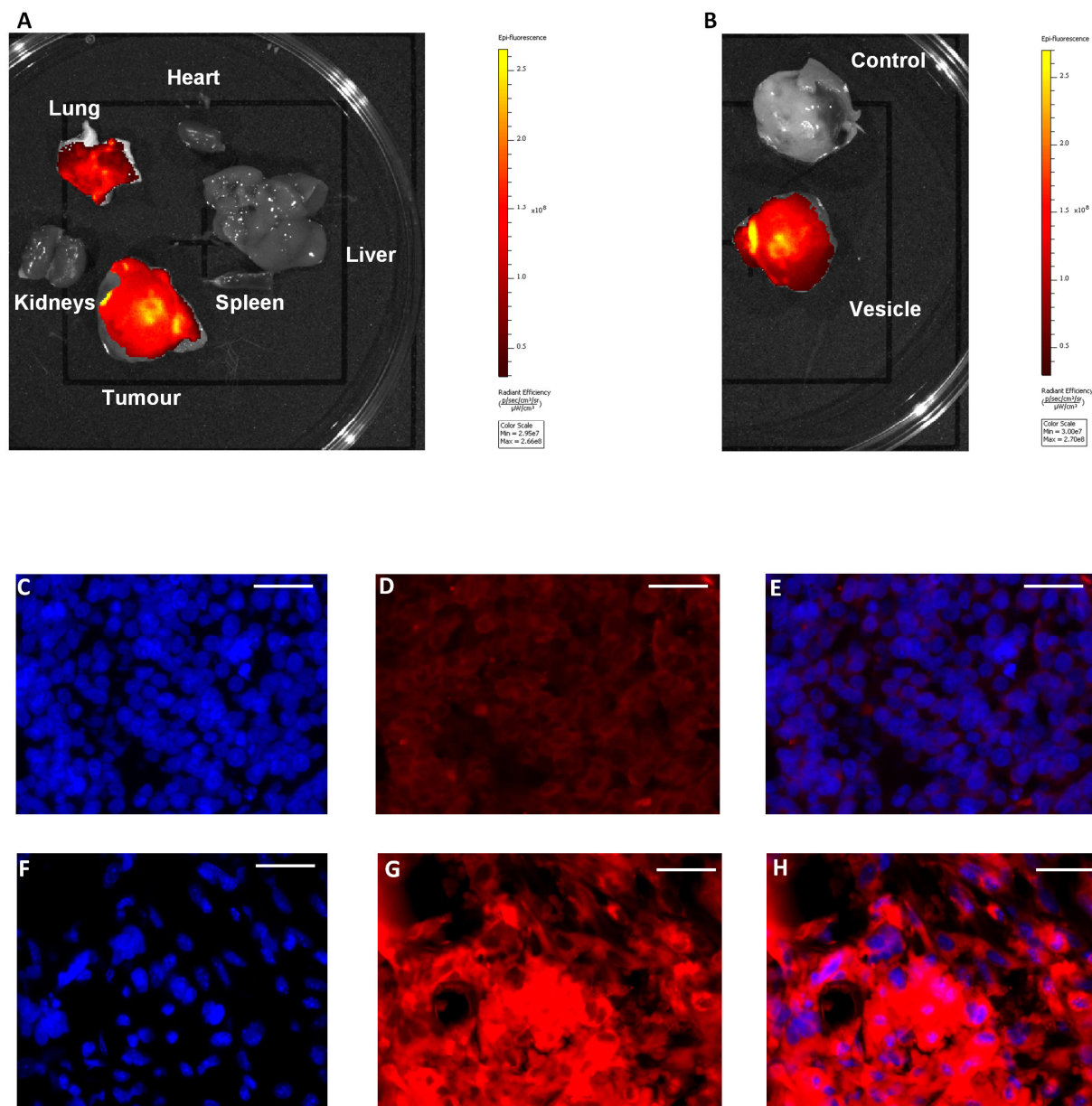




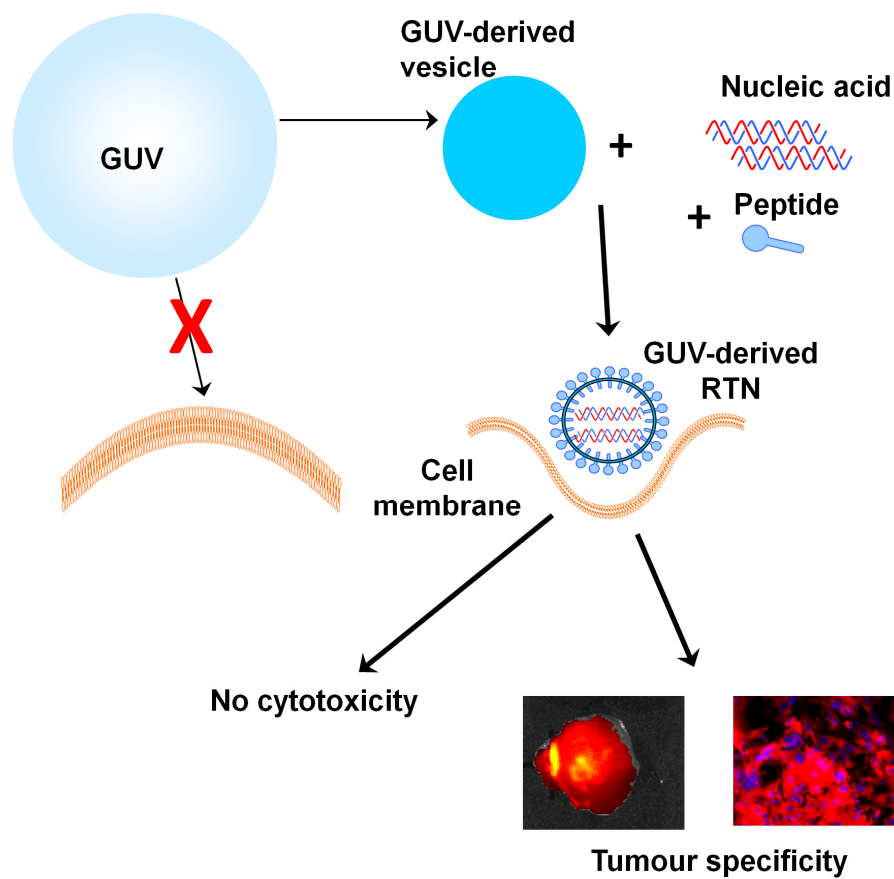
A**B****C**







862
863



864
865
866 The efficient targeted delivery of nucleic acids *in vivo* provides some of the greatest challenges
867 to the development of genetic therapies. Giant unilamellar lipid vesicles (GUVs) have been used
868 mainly as cell and tissue mimics and are instrumental in studying lipid bilayers and interactions.
869 Here, the GUVs have been modified into smaller nanovesicles. We have then developed novel
870 nanovesicle complexes comprising self-assembling mixtures of the nanovesicles, plasmid DNA
871 or siRNA, and targeting peptide ligands. Their biophysical properties were studied and their
872 transfection efficiency was investigated. They transfected cells efficiently without any associated
873 cytotoxicity and with targeting specificity, and *in vivo* they resulted in very high and tumour-
874 specific uptake and in addition, efficiently transfected the lung. The peptide-targeted nanovesicle
875 complexes allow for the specific targeted enhancement of nucleic acid delivery with improved
876 biosafety over liposomal formulations and represent a promising tool to improve our arsenal of
877 safe, non-viral vectors to deliver therapeutic cargos in a variety of disorders.